

Umklapp Lasing with a Quantum Degenerate Fermi Gas

Francesco Piazza^{1*} and Philipp Strack²

¹Physik Department, Technische Universität München, 85747 Garching, Germany and

² Department of Physics, Harvard University, Cambridge MA 02138

(Dated: September 3, 2022)

We introduce the driven quantum degenerate Fermi gas as a lasing medium in optical cavities. We show that the existence of a Fermi surface fundamentally alters the charge-ordering (“self-organization”) superradiant transition that occurs when the atoms are driven sufficiently strongly. Resonant Umklapp scattering processes, where the fermions are scattered from one side of the Fermi surface to the other by exchanging photon momenta, lead to Peierls reconstruction of the dynamical cavity band structure at low superradiance threshold. The spectral properties of the cavity can be tuned by the Fermi wavevector (the density of the gas) relative to the cavity and pump photon momenta. The cavity spectrum can have broadband features from the fermionic particle-hole continuum as well as frequency ranges with narrow linewidth due to dispersive effects of the Fermi gas.

Lasing [1, 2] and superradiance [3–5] phenomena are currently enjoying a renaissance as research topics in atomic physics. Fundamentally based on the interaction of matter with an electromagnetic (light) field, the atomic dipoles in a “lasing medium” collectively emit into selected modes of the electromagnetic field and thereby create an amplified and coherent source of light. Present-day lasers use different types of gain media and cover a wide range of output frequencies for application in both, fundamental research and industry.

A recent string of papers has reported on superradiance [6, 7] and lasing-type instabilities using Bose gases of various type (thermal atoms [8, 9], photon gases [10] and Bose-Einstein condensed atoms [11–14]) in optical cavities. Buoyed by experimental control over essentially single excitation quanta of atoms and photons [15–19] in cavity quantum electrodynamics, these works offer intriguing prospects for the next wave of experiments on strongly interacting light-matter systems including a new regime where unexpected many-body and quantum fluctuation effects of the lasing medium may become visible. Bohnet *et al.* [20] recently operated a superradiant “bad-cavity” laser in the few-photon regime based on coherent oscillations of the inter-atomic, collective dipole of the ultracold atoms in the cavity [21].

In this paper, we point out that a *quantum degenerate Fermi gas* has remarkable features as a lasing medium in a transversally driven cavity as sketched in Fig. 1. We show that the quantum statistics of the Fermi gas puts the coupled cavity+atoms system generically close to superradiance threshold as a consequence of the Pauli exclusion principle (“Pauli pressure”). Physically, this arises from enhanced scattering of fermions between different points on the Fermi surface with radius $|k_F|$ by exchanging relatively large photon momenta \mathbf{Q} from the cavity as illustrated in Fig. 1. By changing the power of the pump laser at a given density of the Fermi gas, the lasing transition is concomitant with the spontaneous formation of a charge density wave oscillating with $1/Q$ in real space. Tuning the ratio $|k_F|/|Q|$ allows to generate a cavity spectrum with “broadband light” in certain spectral ranges or, for energies outside the particle-hole continuum of the fermions, light with relatively narrow linewidth. The normal mode splitting of the cavity by a single atom is completely replaced by many-body

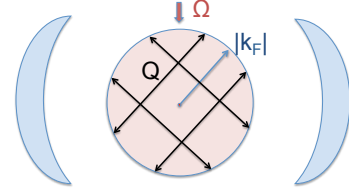


FIG. 1. Fermi sphere (red circle) inside the mirrors of an optical cavity (curved, blue) in combined position-momentum representation. $|k_F|$ is the Fermi momentum and \mathbf{Q} is the superposition of the cavity momentum and the momentum of pump laser with amplitude Ω . The essential physics exploited in this paper are Umklapp scattering events where fermionic atoms are scattered from one side of the Fermi surface to the other by exchanging photon momenta \mathbf{Q} .

effects for which the quantum statistics of the fermions plays a critical role. With a focus on different aspects, fermions in optical cavities were considered previously in Refs. 22–24.

In one dimensional metals, where weakly interacting electrons move in a lattice of ions, the lowering of total energy by spontaneous breaking of translational symmetry, that turns the metal into an insulator by gapping out the Fermi points, was first discussed by Peierls many years ago [25]. In solid state materials, the ions are so much heavier than the electrons, that one can regard the ion potential as static and conservative and essentially ignore the ion dynamics completely (the same is true for conventional optical lattices [26]).

A key difference of cavity-generated dynamical optical potentials in the strong-coupling regime is the backaction of the atomic motion onto the dynamics of the light-field [19] and vice versa, which, combined with the quantum statistical properties of the Fermi gas, ultimately lead to the Dicke-Peierls Instability (DPI) discussed in the present paper. In contrast to self-organization transitions using bosons or (effective) spins [27–51], our DPI is strongly dimensionality-dependent: in 1d, the Fermi gas can charge-order into a superradiant Peierls insulator (SPI) characterized by an excitation (charge) gap already at very low threshold. For 2- and 3d traps, effective Fermi landscapes pierced by “hole and electron pockets” with gapless fermion excitations, termed superradiant charge-ordered Fermi liquid (SCOFL), appear.

We consider N spinless fermionic atoms with two internal electronic levels trapped inside a transversally driven cavity. The quantized excitations of the coupled atoms plus driven cavity system will be described in terms of the field operators $\hat{\psi}_{g/e}$ for the atoms in the internal ground or excited state and the annihilation operator \hat{a} for a cavity photon [37]. The atomic operators obey fermionic quantum statistics and fulfill the (anti-) commutation relation $\{\hat{\psi}(\mathbf{r}), \hat{\psi}^\dagger(\mathbf{r}')\} = \delta_{\mathbf{r},\mathbf{r}'}$. In a frame rotating with the frequency ω_p of the pump laser the Hamiltonian $\hat{H} = \hat{H}_a + \hat{H}_c + \hat{H}_{a/c} + \hat{H}_{a/p}$ contains four terms: $\hat{H}_c = -\Delta_c \hat{a}^\dagger \hat{a}$ and

$$\begin{aligned}\hat{H}_a &= \int d\mathbf{r} \left[\hat{\psi}_g^\dagger(\mathbf{r}) \left(-\frac{\nabla^2}{2m} \right) \hat{\psi}_g(\mathbf{r}) + \hat{\psi}_e^\dagger(\mathbf{r}) \left(-\frac{\nabla^2}{2m} - \Delta_a \right) \hat{\psi}_e(\mathbf{r}) \right] \\ \hat{H}_{a/c} &= -i g_0 \int d\mathbf{r} \hat{\psi}_g^\dagger(\mathbf{r}) \eta_c(\mathbf{r}) \hat{a}^\dagger \hat{\psi}_e(\mathbf{r}) + \text{h.c.} \\ \hat{H}_{a/p} &= -i \Omega \int d\mathbf{r} \hat{\psi}_g^\dagger(\mathbf{r}) \eta_p(\mathbf{r}) \hat{\psi}_e(\mathbf{r}) + \text{h.c.}\end{aligned}\quad (1)$$

Here, \hat{H}_a describes the kinetic energy of the atoms with mass m from moving around inside the cavity and the excited state detuning between the pump and the atomic resonance is $\Delta_a = \omega_p - \omega_c$. $\Delta_c = \omega_p - \omega_c$ is the detuning between the pump and the cavity mode and Ω is the pump Rabi frequency. We operate in the standard regime where the atoms couple to only a single excitation mode of the electromagnetic field of the cavity with single-photon Rabi coupling g_0 . The functions $\eta_c(\mathbf{r}) = \cos(\mathbf{Q}_c \cdot \mathbf{r})$ and $\eta_p(\mathbf{r}) = \cos(\mathbf{Q}_p \cdot \mathbf{r})$ contain the spatial structure of the mode functions of the (standing-wave) cavity light field and the pump laser, respectively. In the following, we neglect the spontaneous emission from the excited atomic level by assuming that the detuning Δ_a be by far the largest energy scale. This allows us to adiabatically eliminate the excited atomic level. We will further assume that the atom-cavity system can deposit photons and energy from the pump laser into the bath of electromagnetic modes outside the cavity without incurring noise-induced fluctuation terms. This is expected to yield the qualitatively new features of the phase diagram and the cavity photon spectrum since in the present setup we have a clear separation between the cavity energy scale Δ_c, κ (typically MHz) and the atomic scale μ, E_R (typically KHz), where κ is the photon loss rate, μ is the chemical potential of the atoms and E_R is the cavity recoil energy.

We proceed by generalizing our recently developed formalism to include spatially varying pump laser potential [54]. We map the Hamiltonian (1) to an effective action using an infinite-dimensional atomic Bloch vector $\Psi^T(\mathbf{k}) = (\psi_{k_x, k_y}, \psi_{k_x - Q_x, k_y}, \psi_{k_x + Q_x, k_y}, \psi_{k_x, k_y - Q_y}, \psi_{k_x, k_y + Q_y}, \psi_{k_x - Q_x, k_y - Q_y}, \dots)$ that exhaustively divides momentum space into cavity-generated “bands” differentiated by multiples of cavity momentum $\mathbf{Q}_c = (Q_x, 0)$ in x -direction and multiples of the pump laser momentum $\mathbf{Q}_p = (0, Q_y)$ in the y -direction transversal to the cavity axis. Q_x and Q_y need not be equal. The momentum sums are now restricted to the first Brillouin zone $\mathbf{k} \in \mathcal{B}$, i. e. $\mathbf{k} = (-Q_x/2 < k_x < Q_x/2, -Q_y/2 < k_y < Q_y/2)$. We now first eliminate the atomic excited state adiabatically and

then integrate out the atomic ground state to arrive at the photon-only action:

$$S_{\text{eff}}[a^*, a] = \frac{1}{\beta} \sum_n (-i\omega_n - \Delta_c) |a_n|^2 - \text{Tr} \ln [M_{n,m}(\mathbf{k})], \quad (2)$$

with $\text{Tr} = \sum_n L^d \int_{\mathcal{B}} \frac{d\mathbf{k}}{(2\pi)^d} \text{tr}$, where tr is matrix trace in Nambu space over the formally infinite-dimensional matrix $M_{n,m}(\mathbf{k})$. The matrix (given explicitly in the Supplemental Material) is symmetric and contains all the scattering processes between fermions and photons. On its diagonal are the fermion propagators evaluated at the momenta corresponding to the different cavity-generated Bloch bands, $G_F^{-1}[i, j] = \beta \delta_{n,m} (-i\nu_n + \xi_{\mathbf{k}}[i, j])$. Additionally, there is an additional spatial modulation of the chemical potential induced by the cavity field, as well as a Stark shift from the pump. The fermion dispersion relative to the chemical potential is

$$\xi_{\mathbf{k}}[i, j] = \frac{(k_x + iQ_x)^2 + (k_y + jQ_y)^2}{2m} - \mu_\psi, \quad (3)$$

where i and j are integers standing for the multiples of cavity and/or pump momenta the photons can transfer to the atoms. In the Supplementary Material, we derive the “dual” effective action to Eq. (2) formulated entirely in terms of collective density fields of the fermionic atoms.

All our results can be obtained from a careful analysis of Eq. (2). We begin by presenting the phase diagram upon varying the pump strength Ω as a function of the fermion density n_ψ and for different temperatures T . This can be obtained by a saddle-point analysis of the action (2) at fixed density $n_\psi = N/L^d$, as done in [54]. The corresponding mean-field solution $a_n = \beta \delta_{n,0} \sqrt{N} \alpha$ becomes exact in the thermodynamic limit $N, L \rightarrow \infty, n_\psi = \text{const.}$

The phase diagram for the $d = 1$ case, when the fermionic atoms are tightly confined in tubes parallel to the cavity axis so that the two-photon momentum transfer $\mathbf{Q} = \mathbf{Q}_x + \mathbf{Q}_y \simeq \mathbf{Q}_x$, is shown in Fig. 2. The critical pump strength Ω_D above which the system is self-organised/superradiant strongly depends on the fermion density or, equivalently, on the 1D Fermi momentum $k_F^{1D} = \pi n_\psi$. In particular, we notice a strong suppression of Ω_D when $k_F^{1D} \simeq Q/2$. This condition indeed implies that a cavity photon can scatter an atom from the Fermi surface (for $d = 1$ Fermi points) at very low energy cost with a momentum transfer \mathbf{Q} which inverts the direction of the atomic motion (Umklapp scattering). This condition corresponds to the Fermi surface crossing the Bragg plane (point in $d = 1$) separating the first and second Brillouin zone in the reciprocal lattice with lattice vector equal to the momentum transfer [55]. For fermions in $d = 1$, the system becomes unstable towards superradiance even at infinitesimal pump strength for $T = 0$ and $k_F^{1D} = Q/2$. The $T = 0$ line in Fig. 2 goes indeed to zero like $1/\ln|1 - Q/2k_F|^{-1}$, while as soon as a small finite temperature (also potentially induced by cavity decay) is present Ω_D stays finite. This is analogous to the Peierls instability present in one-dimensional metals [25], where it becomes energetically favorable for the electrons to break the

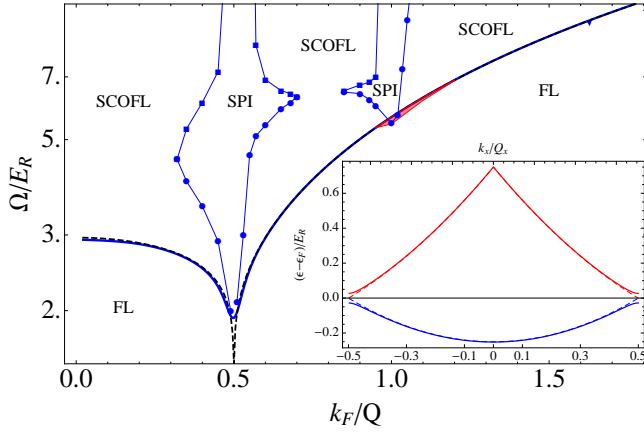


FIG. 2. Phase diagram for a one-dimensional Fermi gas in an optical cavity as a function of Fermi- (k_F) over cavity ($Q = \sqrt{2mE_R}$) momentum versus pump amplitude Ω . Inset shows gap opening at the Fermi points. Temperatures are $k_B T = 0$ (black-dashed line), $k_B T = 0.01E_R$ (blue-solid line). At $Q = 2k_F$ the system is perfectly nested and Peierls reconstruction into a superradiant Peierls insulator (SPI) sets in at relatively small Ω . Away from nesting the Z_2 charge symmetry breaking leads to a superradiant charge-ordered Fermi liquid (SCOFL). The red-shaded area extending from the second order transition line indicates the hysteresis region preceding the first-order phase transition from the Fermi liquid (FL) into the SPI at $k_F/Q = 1$; there the Fermi energies lies in the band between the second and third cavity generated bands. The remaining parameters are $\Delta_c = -0.2E_R$, $Ng_0^2/\Delta_a = -0.05E_R$, $g_0/\Delta_a = -0.1$.

discrete translational symmetry by doubling the lattice period so that the Fermi points get gapped out with the important difference that here the cavity generated lattice does not reorganize but rather first appears due to the instability. Ref. 52 is a related proposal to simulate Peierls physics with hybrid ultracold atom and ion systems. We note that a bosonic, superradiant Mott insulator has recently been obtained by coupling a two-band Bose Hubbard model to a light field [53]. Our system becomes insulating in the superradiant phase for nearly commensurate densities $k_F^{\text{1D}} \approx j Q/2$ (with j integer) as is shown for $j = 2$ in Fig. 2. The superradiant Peierls insulating regions are separated by crossover lines from regions where the system shows superradiant charge order but is still metallic, since the Fermi energy does not lie within the band gap. The FL-SCOFL transition is always continuous except from a region around $k_F \approx Q$ where the transition is first order. The red-shaded area in Fig. 2 shows the region where the free energy has two local minima as a function of the order parameter α . This hysteresis region appears for Ω slightly lower than Ω_D and ends exactly at Ω_D , where the free energy has only a single minimum at finite α , corresponding to the jump in the cavity occupation. We point out that, due to the fact that the atoms couple to a single cavity mode extending all over the cloud, there is no coexistence between the normal and superradiant phase despite hysteresis.

In two dimensions the physics is richer since the spatial structure of the pump laser cannot be neglected. This has two main effects: i) even in the normal phase, by increasing the

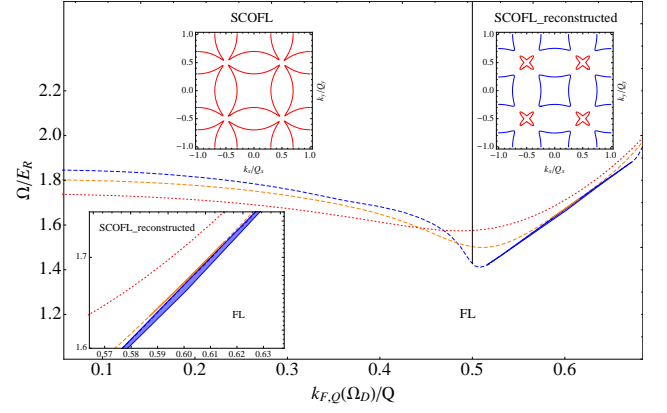


FIG. 3. Phase diagram for a two-dimensional Fermi gas in an optical cavity for $Q_x = Q_y = \sqrt{2mE_R}$. The lines indicate the critical value of the pump strength above which the system is superradiant as a function of the Fermi momentum and for different temperatures: $k_B T = 0.01E_R$ (blue-dashed line), $k_B T = 0.05E_R$ (orange-dashed line), and $k_B T = 0.1E_R$ (red-dotted line). The lower inset shows an enlargement of the region where the transition is first order, as indicated by the shaded area, corresponding to the hysteresis region, extending from the second order transition line. The vertical dashed line separates the two different superradiant regimes with topologically trivial Fermi surface and reconstructed Fermi surface, as illustrated in the two upper insets: left at $k_F \hat{Q}(\Omega_D) = 0.49Q$, $\alpha = 0.1$, right $k_F \hat{Q}(\Omega_D) = 0.53Q$, $\alpha = 0.2$. Here the Fermi surface is shown in the repeated-zone scheme relative to the Brillouin zone \mathcal{B} . Purple lines delimit “electron” pockets with occupied levels while blue lines delimit hole pockets with empty levels. The remaining parameters are the same as in Fig. 2.

pump strength we deform the Fermi surface of the atoms inside the pump lattice with vector \mathbf{Q}_p , ii) the density wave in the superradiant phase has momentum $\mathbf{Q} = \mathbf{Q}_c + \mathbf{Q}_p$, corresponding to a checkerboard lattice with reciprocal vector \mathbf{Q} whose length is $Q = \sqrt{Q_x^2 + Q_y^2}$ [55]. The phase diagram for different temperatures as a function of the Fermi momentum along the \mathbf{Q} direction calculated at the critical pump strength $k_F \hat{Q}(\Omega_D)$ is presented in Fig. 3. As in the $d = 1$ case, we observe a suppression of Ω_D for $k_F \hat{Q}(\Omega_D) \approx Q/2$, marked by the vertical black-dashed line in Fig. 3. The suppression of Ω_D is much weaker as compared to $d = 1$ since perfect nesting is absent. Again, the minimum in Ω_D is at $k_F \hat{Q}(\Omega_D) \approx Q/2$, where this time the Fermi momentum depends on the pump strength due to the deformation of the Fermi surface discussed at i). Therefore, Q has to be compared with $k_F(\Omega)$ at the critical point $\Omega = \Omega_D$ and the direction along \mathbf{Q} (actually any of the four orthogonal ones) is the one relevant for nesting. In Fig. 3, the minimum is not exactly at $k_F \hat{Q}(\Omega_D) = Q/2$ since $T \neq 0$. On the other hand, the two-dimensional checkerboard lattice can lead to reconstruction of the Fermi surface for $k_F \hat{Q}(\Omega_D) > Q/2$, an example of which is given in the right upper inset of Fig. 3. By entering the self-organized phase the atoms change from a simply connected Fermi surface to one consisting of separated closed surfaces delimiting zones with occupied and empty states. The blue Fermi surface belongs

to the first lattice band while the red surface to the second higher band. The condition $k_F \hat{Q}(\Omega_D)$ implies that the Fermi surface has to intersect the first Bragg plane of the reciprocal chequerboard lattice [55]. In contrast to the one-dimensional case, in $d = 2$ the atomic medium is therefore always metallic in the superradiant phase. The order of the superradiant transition depends on $k_F \hat{Q}(\Omega_D)$ and temperature. As can be seen from Fig. 3, there is a large region where the transition is first order and hysteresis is present (indicated by the shaded area). The range of densities for which the transition is first order corresponds to the region where Ω_D depends linearly on $k_F \hat{Q}(\Omega_D)$ and gets smaller with increasing temperature (see lower inset in Fig. 3). In two dimensions, the Fermi momentum is determined by the density and mass of the fermions as $|\mathbf{k}_F| = \sqrt{4\pi n_\psi}$. The cavity momentum is determined by the (wave-) length of the cavity $Q_x = 2\pi/\lambda$ with λ an optical wavelength for example ~ 800 nm. So, for a degenerate Fermi gas at densities around $10^{14} - 10^{15} \text{ m}^{-2}$ the various regimes we are discussing are experimentally accessible.

The cavity photon spectrum can be obtained exactly in closed form in terms of the density response function ("particle-hole bubble") of the Fermi gas at finite (cavity) momentum $\Sigma(\omega) = -\frac{\lambda^2}{2n} \Pi_F(\omega, \mathbf{Q})$:

$$A(\omega) = \frac{-2(\delta_c + \omega)^2 \text{Im}\Sigma(\omega)}{(\delta_c^2 - \omega^2 + 2\delta_c \text{Re}\Sigma(\omega))^2 + (2\delta_c \text{Im}\Sigma(\omega))^2}, \quad (4)$$

where $\lambda = \Omega_{g0}/\Delta_a$. Explicit formulae for $\Pi_F(\omega, \mathbf{Q})$ are given in the Supplemental Material. We will focus on the zero temperature case in $d = 1$ at $k_F/Q = 0.4$ slightly left of the "dip" in Fig. 2 and compare it to the perfectly nested case $k_F/Q = 0.5$. For energies within the particle-hole continuum, $(Q/k_F)^2 - 2Q/k_F \leq \omega/\epsilon_F \leq (Q/k_F)^2 + 2Q/k_F$, the broadening of the photon spectrum is determined by a *frequency independent* constant

$$\text{Im}\Sigma(\omega)_{1d} = -\frac{\lambda^2 \pi k_F}{8\epsilon_F Q}. \quad (5)$$

Instead of normal-mode split double peak in the cavity spectrum, Fig. 4 exhibits a broad continuum with discontinuities at the edges of the particle-hole continuum. Outside the particle-hole continuum, $\text{Im}\Sigma(\omega) = 0$ and the cavity spectrum is dominated by a sharp peak $A(\omega) = (1 + \delta_c \text{Re}\Sigma(\omega = E)) \pi \delta(\omega - E)$ at the "soft mode" energy E , which close to the critical point is $E \simeq \sqrt{\delta_c^2 + 2\delta_c \text{Re}\Sigma(\omega = 0)}$. In Fig. 4 the sharp soft mode peak is illustrated with an upward pointing arrow to the left of the continuum. The fermionic particle-hole excitations may be viewed as a spectator quantum-critical continuum which damps the photon dynamics; its onset, however, is independent of the coupling to the cavity. In addition, and differently from the Bose gas [54], away from the nested case $Q = 2k_F$ the cavity spectrum at low frequencies close to the DPI transition remains undamped and sharply defined. Inclusion of finite cavity decay rate κ could in general modify this. However, in recent experiments κ is $\sim \text{MHz}$ and ~ 3 orders of magnitude larger than the characteristic kHz energies from the atomic

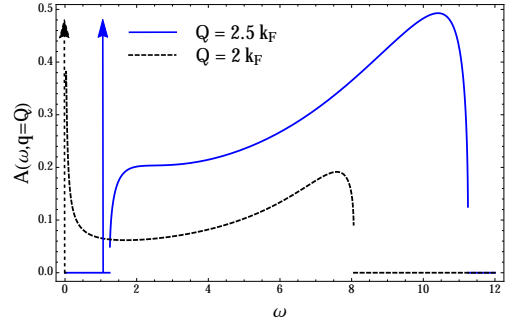


FIG. 4. Cavity photon spectrum when approaching the $T = 0$ Dicke-Peierls instability in one dimension. The black-dashed curve describes the perfectly nested case in which the fermionic particle-hole continuum reaches down to zero frequency and the critical pump strength is zero. The upward arrows denote the sharp δ -function peaks at the frequency of the soft mode, which move toward $\omega = 0$ for $\lambda \rightarrow \lambda_D$. The linewidth of the cavity light is therefore strongly frequency dependent; within the particle-hole continuum, there is "broadband" emission for a range of frequencies, outside of the particle-hole continuum, the linewidth is very narrow. This features are expected to be universal properties of the Fermi gas as a lasing medium and as such present also in $d = 2, 3$. Frequencies ω are given in units of the Fermi energy ϵ_F and momenta in units of the Fermi momentum k_F . Numerical parameters here are chosen close to threshold, $n=1$, $\lambda = 0.98\lambda_D$.

motion. The broadening [13, 14] observed was only of the order of kHz suggesting that the fundamental limits to the cavity linewidth arise from the atomic motion; this also happens in the bad cavity lasing regime, where the cavity linewidth is orders of magnitudes smaller than κ [20, 21].

In summary, we discussed charge ordering instabilities of a quantum degenerate Fermi gas induced by the vacuum field of an electromagnetic resonator. We showed that the quantum statistics of the Fermi gas has striking effects on both, the threshold properties of the driven atoms+cavity system as well as the light emitted from it. Unique applications of our results include searching for narrow linewidth lasers [21, 57] and studying pairing instabilities of *interacting* Fermi gases with reconstructing Fermi surfaces; this may offer prospects of a new platform for quantum simulation of high-temperature superconductors [58].

Acknowledgments – We are grateful to W. Zwerger for collaboration and guidance on related work, and to M. D. Lukin for insightful discussions and references on lasing. This work was supported by the Alexander Von Humboldt foundation, the DFG under grant Str 1176/1-1, by the NSF under Grant DMR-1103860, by the Templeton foundation, by the Center for Ultracold Atoms (CUA), and by the Multidisciplinary University Research Initiative (MURI).

* francesco.piazza@ph.tum.de

[1] A. E. Siegman, *Lasers*, University Science Books (1986)

[2] H. Haken, *Light, Vol. 2, Laser Light Dynamics*, North-Holland

- Physics Publishing (1985)
- [3] R. H. Dicke, Phys. Rev. **93**, 99 (1954)
 - [4] M. Gross and S. Haroche, Phys. Reports **93**, 301 (1982)
 - [5] Y. Yamamoto, and A. Imamoglu, *Mesoscopic Quantum Optics*, J. Wiley & Sons, Inc. (1999)
 - [6] S. Inouye, *et al.*, Science **285**, 571 (1999)
 - [7] Y. Yoshikawa, Y. Torii, and T. Kuga, Phys. Rev. Lett. **94**, 083602 (2005)
 - [8] A. T. Black, H. W. Chan, and V. Vuletić, Phys. Rev. Lett. **91**, 203001 (2003)
 - [9] S. Slama, *et al.*, Phys. Rev. Lett. **98**, 053603 (2007)
 - [10] J. Klaers, J. Schmitt, F. Vewinger, and M. Weitz, Nature **468**, 545 (2010)
 - [11] K. Baumann, C. Guerlin, F. Brennecke, and T. Esslinger, Nature **464**, 1301 (2010)
 - [12] K. Baumann, R. Mottl, F. Brennecke, and T. Esslinger Phys. Rev. Lett. **107**, 140402 (2011)
 - [13] R. Mottl, *et al.*, Science **336**, 1570 (2012)
 - [14] F. Brennecke, *et al.*, arXiv:1304.4939v1
 - [15] R. J. Thompson, G. Rempe, and H. J. Kimble, Phys. Rev. Lett. **68**, 1132 (1992)
 - [16] R. Miller, T. E. Northup, K. M. Birnbaum, A. Boca, A. D. Boozer, and H. J. Kimble, J. Phys. B: At. Mol. Opt. Phys. **38**, 551 (2005).
 - [17] S. Haroche, and J. M. Raimond, *Exploring the Quantum: Atoms, Cavities, and Photons*, Oxford University Press (2006)
 - [18] H. Walther, B. T. H. Varcoe, B.-G. Englert, and T. Becker, Rep. Prog. Phys. **69**, 1325 (2006).
 - [19] H. Ritsch, P. Domokos, F. Brennecke, and T. Esslinger, Rev. Mod. Phys. **85**, 553 (2013)
 - [20] J. G. Bohnet, Z. Chen, J. M. Weiner, D. Meiser, M. J. Holland, and J. K. Thompson, Nature **78** 484 (2012)
 - [21] D. Meiser, J. Ye, D. R. Carlson, and M. J. Holland, Phys. Rev. Lett. **102**, 163601 (2009)
 - [22] J. Larson, B. Damski, G. Morigi, M. Lewenstein, Phys. Rev. Lett. **100**, 050401 (2008)
 - [23] R. Kanamoto, and P. Meystre, Phys. Rev. Lett. **104**, 063601 (2010)
 - [24] M. Müller, P. Strack, and S. Sachdev, Phys. Rev. A **86**, 023604 (2013)
 - [25] R. E. Peierls, *Quantum theory of solids*, Clarendon, Oxford (1955).
 - [26] I. Bloch, J. Dalibard and W. Zwerger, Rev. Mod. Phys. **80**, 885 (2008)
 - [27] K. Hepp, and E. H. Lieb, Ann. of Phys. **76**, 360 (1973)
 - [28] Y. K. Wang, and F. T. Hioe, Phys. Rev. A **7**, 831 (1973)
 - [29] R. Bonifacio, and L. De Salvo, Nucl. Instrum. Methods **341**, 360 (1994)
 - [30] P. Domokos, and H. Ritsch, Phys. Rev. Lett. **89**, 253003 (2002)
 - [31] C. Emary and T. Brandes, Phys. Rev. E **67**, 066203 (2003)
 - [32] N. Lambert, C. Emary, and T. Brandes, Phys. Rev. Lett. **92**, 073602 (2004)
 - [33] J.K.Asbóth, P.Domokos, H.Ritsch, and A.Vukics, Phys.Rev. A **72**, 053417 (2005)
 - [34] D. Nagy, J. K. Asbóth, P. Domokos, and H. Ritsch, Europhys. Lett. **74**, 254 (2006)
 - [35] A. Vukics, C. Maschler, and H. Ritsch, New J. Phys. **9**, 255 (2007)
 - [36] F. Dimer, *et al.*, Phys. Rev. A **75**, 013804 (2007)
 - [37] C. Maschler, I. Mekhov, and H. Ritsch, EPJD **46**, 545 (2008)
 - [38] D. Nagy, G. Szirmai, and P. Domokos, EPJD **48**, 127 (2008)
 - [39] J. Larson, and M. Lewenstein, NJP **11**, 063027 (2009)
 - [40] D. Nagy, G. Konya, G. Szirmai, and P. Domokos, Phys. Rev. Lett. **104**, 130401 (2010)
 - [41] S. Gopalakrishnan, B. L. Lev, and P. M. Goldbart, Phys. Rev. A **82**, 043612 (2010)
 - [42] S.F. Vidal, G. De Chiara, J. Larson, G. Morigi, Phys. Rev. A **81**, 043407 (2010)
 - [43] J. Keeling, M.J. Bhaseen, B.D. Simons, Phys. Rev. Lett. **105**, 043001 (2010)
 - [44] G. Konya, G. Szirmai, and P. Domokos, EPJD **65**, 33 (2011)
 - [45] D. Nagy, G. Szirmai, and P. Domokos, Phys. Rev. A **84**, 043637 (2011)
 - [46] B. Öztop, M. Bordyuh, O. E. Müstecaplıoglu, and H. E. Türeci, New J. Phys. **14**, 085011 (2012)
 - [47] E. G. Dalla Torre, *et al.* Phys. Rev. A **87**, 023831 (2012)
 - [48] M. J. Bhaseen, J. Mayoh, B. D. Simons, and J. Keeling, Phys. Rev. A **85**, 013817 (2012)
 - [49] D. E. Chang, J. I. Cirac, and H. J. Kimble, Phys. Rev. Lett. **110**, 113606 (2013)
 - [50] Y. Li, L. He, and W. Hofstetter, Phys. Rev. A **87**, 051604 (2013)
 - [51] B. Oeztop, M. Kulkarni, and H. E. Türeci, arXiv:1306.3889 (2013)
 - [52] U. Bissbort *et al.*, Phys. Rev. Lett. **111**, 080501 (2013)
 - [53] A. O. Silver, M. Hohenadler, M. J. Bhaseen, and B. D. Simons, Phys. Rev. A **81**, 023617 (2010)
 - [54] F. Piazza, P. Strack and W. Zwerger, Ann. of Phys. **339**, 135 (2013)
 - [55] See supplementary material.
 - [56] N. W. Ashcroft, and N. D. Mermin, *Solid State Physics*, Thomson Learning (1976)
 - [57] M. D. Lukin, *et al.*, Phys. Rev. Lett. **79**, 2959 (1997).
 - [58] M. Vojta, Physica C **481**, 178 (2012)
 - [59] H. Fukuyama, Y. Hasegawa, and O. Narikiyo, Journal of the Physics Society of Japan, **60**, 2013 (1991)
 - [60] P.-A. Bares and X.-G. Wen, Phys. Rev. B **48**, 8636 (1993).
 - [61] W. Metzner, C. Castellani, and C. Di Castro, Adv. in Phys. **47**, 317 (1998).
 - [62] B. Mihalla, arXiv:1111.5337 (2011).

Supplemental Material

Explicit form of Nambu matrix $M_{n,m}(\mathbf{k})$

The Nambu matrix $M_{n,m}(\mathbf{k})$ used in Eq. (2) in the main text reads

$$M_{n,m}(\mathbf{k}) = \begin{pmatrix} G_\psi^{-1}[0,0] & 0 & 0 & 0 & 0 & \Lambda_{n,m}/2 & \Lambda_{n,m}/2 & \Lambda_{n,m}/2 & \Lambda_{n,m}/2 & U_{n,m}/2 & \dots \\ 0 & G_\psi^{-1}[-1,0] & U_{n,m}/2 & \Lambda_{n,m}/2 & \Lambda_{n,m}/2 & 0 & 0 & 0 & 0 & 0 & \\ 0 & U_{n,m}/2 & G_\psi^{-1}[1,0] & \Lambda_{n,m}/2 & \Lambda_{n,m}/2 & 0 & 0 & 0 & 0 & 0 & \\ 0 & \Lambda_{n,m}/2 & \Lambda_{n,m}/2 & G_\psi^{-1}[0,-1] & U_\Omega/2 & 0 & 0 & 0 & 0 & 0 & \\ 0 & \Lambda_{n,m}/2 & \Lambda_{n,m}/2 & U_\Omega/2 & G_\psi^{-1}[0,1] & 0 & 0 & 0 & 0 & 0 & \\ \Lambda_{n,m}/2 & 0 & 0 & 0 & 0 & G_\psi^{-1}[-1,-1] & U_\Omega/2 & U_{n,m}/2 & 0 & \Lambda_{n,m}/2 & \\ \Lambda_{n,m}/2 & 0 & 0 & 0 & 0 & U_\Omega/2 & G_\psi^{-1}[-1,-1] & 0 & U_{n,m}/2 & \Lambda_{n,m}/2 & \\ \Lambda_{n,m}/2 & 0 & 0 & 0 & 0 & U_{n,m}/2 & 0 & G_\psi^{-1}[-1,1] & U_\Omega/2 & 0 & \\ \Lambda_{n,m}/2 & 0 & 0 & 0 & 0 & 0 & U_{n,m}/2 & U_\Omega/2 & G_\psi^{-1}[1,1] & 0 & \\ U_{n,m}/2 & 0 & 0 & 0 & 0 & \Lambda_{n,m}/2 & \Lambda_{n,m}/2 & 0 & 0 & G_\psi^{-1}[-2,0] & \\ \vdots & & & & & & & & & & \ddots \end{pmatrix}, \quad (6)$$

where $\Lambda_{n,m} = (g_0\Omega/\Delta_a)(a_{m-n}^* + a_{n-m})$, $U_{n,m} = (g_0^2/2\beta\Delta_a) \sum_{n_1} a_{n_1-n}^* a_{n_1-m}$, and $U_\Omega = \beta\Omega^2/2\Delta_a$. The diagonal entries are the fermion propagators $G_\psi^{-1}[i,j] = \beta\delta_{n,m}(-i\nu_n + \xi_{\mathbf{k}}[i,j]) + U_{n,m} + U_\Omega$. We indicate bosonic and fermionic Matsubara frequencies by $\omega_n = \pi 2n/\beta$ and $\nu_n = \pi(2n+1)/\beta$, respectively. In our numerical computations, this matrix is truncated well in the regime where results converge.

Dual effective action for fermionic atoms

We here derive the dual effective action for the ground state fermionic atoms. After elimination of the excited, internal state the action corresponding to the Hamiltonian in Eq. (1) of the main text reads

$$\begin{aligned} S_{\psi\psi} &= T \sum_n \int d\mathbf{r} \bar{\psi}_{\mathbf{r}}(\omega) \left\{ -i\omega_n - \frac{\nabla^2}{2m} + \frac{\Omega^2}{\Delta_a} - \mu_\psi \right\} \psi_{\mathbf{r}}(\omega) \\ S_{aa} &= \int_0^\beta d\tau a^*(\tau) \frac{da(\tau)}{d\tau} - \Delta_c a^*(\tau) a(\tau) \\ S_{\psi a} &= \int_0^\beta d\tau \int d\mathbf{r} \bar{\psi}_{\mathbf{r}}(\tau) \psi_{\mathbf{r}}(\tau) \left\{ \frac{(g_0\eta_{\mathbf{r}})^2}{\Delta_a} a^*(\tau) a(\tau) + \frac{\Omega g_0 \eta_{\mathbf{r}}}{\Delta_a} [a(\tau) + a^*(\tau)] \right\}, \end{aligned} \quad (7)$$

where we have used $\eta_{\mathbf{p}}(\mathbf{r}) = 1$, i.e. we here neglect the spatial structure of the pump laser and we dropped the cavity subscript on the cavity mode profile $\eta_{\mathbf{r}}$. We integrate out the photons and get

$$S[\bar{\psi}, \psi] = T \sum_{n,\mathbf{k}} \bar{\psi}_{\mathbf{k}}(\omega) \{ -i\omega_n + \xi_{\mathbf{k}} \} \psi_{\mathbf{k}}(\omega) - \frac{1}{2} \int_0^\beta d\tau \int_0^\beta d\tau' \int d\mathbf{r} \int d\mathbf{r}' n_{\mathbf{r}}^{(\psi)}(\tau) \left(\frac{\Omega g_0}{\Delta_a} \eta_{\mathbf{r}} \right) \mathcal{G}(\tau - \tau') \left(\frac{\Omega g_0}{\Delta_a} \eta_{\mathbf{r}'} \right) n_{\mathbf{r}'}^{(\psi)}(\tau'). \quad (8)$$

where the fermionic density is $n_{\mathbf{r}}^{(\psi)}(\tau) = \bar{\psi}_{\mathbf{r}}(\tau) \psi_{\mathbf{r}}(\tau)$, the fermion dispersion is $\xi_{\mathbf{k}} = \frac{\mathbf{k}^2}{2m} - \mu$ and as before the standing cavity mode functions given by $\eta_{\mathbf{r}} = \cos(\mathbf{Q}_0 \cdot \mathbf{r})$. The photon kernel mediating the interaction

$$\mathcal{G}(\tau - \tau') = T \sum_n \frac{2\mathcal{N}^{(\psi)}(\Omega) - \Delta_c}{-\Omega_n^2 + (\mathcal{N}^{(\psi)}(\Omega) - \Delta_c)^2} e^{-i\Omega_n(\tau - \tau')}, \quad (9)$$

involves (weighted) spatial averages of the fermionic density fluctuations

$$\mathcal{N}^{(\psi)}(\Omega) = \int_0^\beta d\tau \int d\mathbf{r} n_{\mathbf{r}}^{(\psi)}(\tau) \frac{(g_0\eta_{\mathbf{r}})^2}{\Delta_a} e^{i\Omega_n\tau}. \quad (10)$$

In the limit $\Delta_c \gg \mathcal{N}^{(\psi)}(\Omega)$, the interaction becomes approximately instantaneous in (imaginary) time but remains long-ranged in space. Going now to momentum space for the fields $\psi_{\mathbf{r}}(\tau) = \sum_{\mathbf{k}} \psi_{\mathbf{k}}(\tau) e^{-i\mathbf{k}\mathbf{r}}$, $\bar{\psi}_{\mathbf{r}}(\tau) = \sum_{\mathbf{k}} \bar{\psi}_{\mathbf{k}}(\tau) e^{i\mathbf{k}\mathbf{r}}$ we obtain for the interaction term in Eq. (8)

$$S[\bar{\psi}, \psi] = T \sum_{n, \mathbf{k}} \bar{\psi}_{\mathbf{k}}(\omega) \{-i\omega_n + \xi_{\mathbf{k}}\} \psi_{\mathbf{k}}(\omega) - \frac{V_0}{N} \int_0^\beta d\tau \sum_{\mathbf{k}_1, \mathbf{k}_2} \frac{1}{2} \left[\bar{\psi}(\tau)_{\mathbf{k}_1 - \mathbf{Q}_0} \psi_{\mathbf{k}_1}(\tau) + \bar{\psi}(\tau)_{\mathbf{k}_1 + \mathbf{Q}_0} \psi_{\mathbf{k}_1}(\tau) \right] \frac{1}{2} \left[\bar{\psi}(\tau)_{\mathbf{k}_2 - \mathbf{Q}_0} \psi_{\mathbf{k}_2}(\tau) + \bar{\psi}(\tau)_{\mathbf{k}_2 + \mathbf{Q}_0} \psi_{\mathbf{k}_2}(\tau) \right]. \quad (11)$$

with $\frac{V_0}{N} \equiv \left(\frac{\Omega g_0}{\Delta_c} \right)^2 \frac{1}{\Delta_c}$. This action is now a reduced mean-field model for finite- \mathbf{Q}_0 charge-ordering of the Fermi liquid. Applying the same logic as in Ref. 54, it can be shown that this model is exactly solvable in the thermodynamic limit $N \rightarrow \infty$. The derivation of the free energy density proceeds in a standard way. We first decouple the interaction term with a Hubbard-Stratonovich field conjugate to the fermion bilinear

$$\rho_{\mathbf{Q}_0}(\Omega) \leftrightarrow T \sum_{n, \mathbf{k}} \frac{1}{2} \left[\bar{\psi}_{\mathbf{k} - \mathbf{Q}_0}(\Omega + \omega) \psi_{\mathbf{k}}(\omega) + \bar{\psi}_{\mathbf{k} + \mathbf{Q}_0}(\Omega + \omega) \psi_{\mathbf{k}}(\omega) \right] \quad (12)$$

and we can in the following restrict to the static component of the order parameter field $\rho_{\mathbf{Q}_0}(\Omega) \rightarrow \frac{\delta_{\Omega,0}}{T} \rho$. We now integrate out the fermions and obtain the free energy density

$$\frac{F[\rho]}{N} = \frac{\rho^2}{V_0} - T \sum_n \int_{\mathcal{B}} \frac{d\mathbf{k}}{(2\pi)^d} \text{tr} \ln [\mathcal{M}_\rho(\omega_n; \mathbf{k})] \quad (13)$$

where the fermionic Nambu matrix can be written in the form

$$\mathcal{M}_\alpha(\omega_n; \mathbf{k}) = \begin{pmatrix} \ddots & \vdots & \vdots & \vdots & \vdots & \vdots & \ddots \\ 0 & -\frac{\rho}{2} & -i\omega_n + \xi_{\mathbf{k} - \mathbf{Q}_0} & -\frac{\rho}{2} & 0 & 0 & 0 \\ \ddots & 0 & -\frac{\rho}{2} & -i\omega_n + \xi_{\mathbf{k}} & -\frac{\rho}{2} & 0 & \ddots \\ 0 & 0 & 0 & -\frac{\rho}{2} & -i\omega_n + \xi_{\mathbf{k} + \mathbf{Q}_0} & -\frac{\rho}{2} & 0 \\ \ddots & \vdots & \vdots & \vdots & \vdots & \vdots & \ddots \end{pmatrix} \quad (14)$$

By comparing Eq. (13) to the photon-only action Eq. (2) in the main text we see that charge order parameter ρ is dual to the cavity condensate α . The results for the phase diagram in the main text can also be derived from Eq. (8) and the effective free energy for the atomic density Eq. (2).

Bragg planes of the chequerboard lattice

The density wave in the superradiant phase has momentum $\mathbf{Q} = \mathbf{Q}_c + \mathbf{Q}_p$, corresponding to a chequerboard lattice with reciprocal vector \mathbf{Q} whose length is $Q = \sqrt{Q_x^2 + Q_y^2}$, as depicted in Fig. 5. This standard textbook construction for a regular square lattice [56] allows to understand why a reconstructed Fermi surface appears when $k_F > Q/2$, that is, when the Fermi surface crosses the first Bragg line. Indeed, in this case the fermi surface is split between the first and the second Brillouin zone, creating empty corners in the former and filled arcs in the latter. Slightly after entering the superradiant phase where the chequerboard lattice is weak, small gaps appear at the Bragg planes and the empty corners get separated from the filled arcs to form the “electron and hole pockets” discussed in the text and depicted in the upper right inset of Fig. 3 of the main text. The repeated-zone representation used in the latter can be obtained from the construction of Fig. 5 by i) rejoining the different segments of the each Brillouin zone to form a single whole square Brillouin zone, ii) join equal copies of the whole zone to form the periodic structure. There is, however, a difference between the repeated zone scheme obtained from the above prescription and the repeated zone scheme used in Fig. 3 of the main text. In the latter, the reference Brillouin zone is \mathcal{B} which is a square with side length $Q_x = Q/\sqrt{2}$. On the other hand, in Fig. 5 the Brillouin zone is a square with side length Q .

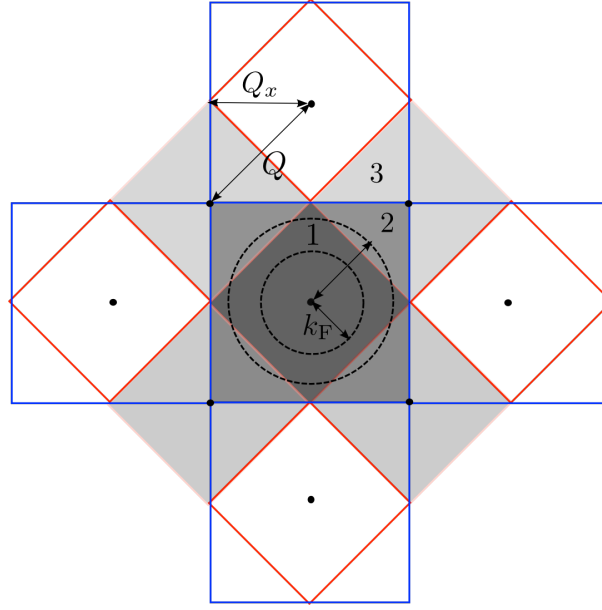


FIG. 5. The reciprocal chequerboard lattice is a regular square lattice with spacing Q separating the lattice points (black circles). The blue and red solid lines correspond to the first two Bragg lines while the shaded areas represent the first three Brillouin zones in different gray scales. The two black-dashed circles show the Fermi surface for two different values of k_F , the larger of which intersects the first Bragg line. Here we took $Q_x = Q_y$ and assumed a circular Fermi surface for simplicity.

Density response of the Fermi gas $\Pi_F(\omega, \mathbf{Q})$

The cavity photon spectrum, Eq. (4) of the main text, can be expressed in completely analytic form in terms of the density response of the Fermi gas evaluated at fixed external momentum \mathbf{Q}

$$\begin{aligned} \Pi_F(\omega_n, \mathbf{Q}) &= \int \frac{d\omega'_n}{2\pi} \int \frac{d^d \mathbf{k}}{(2\pi)^d} G_F(\omega'_n + \omega_n, \mathbf{k} + \mathbf{Q}) G_F(\omega'_n, \mathbf{k}) \\ &= \int \frac{d\omega'_n}{2\pi} \int \frac{d^d \mathbf{k}}{(2\pi)^d} \frac{1}{-i(\omega'_n + \omega_n) + \xi_{\mathbf{k}+\mathbf{Q}}} \frac{1}{-i\omega'_n + \xi_{\mathbf{k}}} \\ &= \int \frac{d^d \mathbf{k}}{(2\pi)^d} \frac{n_F(\xi_{\mathbf{k}+\mathbf{Q}}) - n_F(\xi_{\mathbf{k}})}{\xi_{\mathbf{k}} - \xi_{\mathbf{k}+\mathbf{Q}} - i\omega_n}, \end{aligned} \quad (15)$$

where the Fermi-Dirac distribution function $n_F(x) = \frac{1}{\exp[x/T]+1}$ becomes the standard θ -function at zero temperature $T = 0$. We have added subscript n to the frequency to remind ourselves that ω_n is an imaginary “Matsubara” frequency and that we have not yet analytically continued to real frequencies ω . Note also that Eq. (15) is defined with a relative minus sign with respect to the one-loop Feynman diagram (where an additional minus-sign appears). For rotationally invariant Fermi surfaces, $\xi_{\mathbf{k}} = \frac{k^2}{2m} - \mu$, and a number of analytical expressions are available for the real and imaginary part of $\Pi_F(\omega, \mathbf{Q})$ after analytic continuation to real frequencies ω [59–62].

We give here only the 1d-expressions used to evaluate the cavity photon spectral function Eqs. (4,5) and Fig. 5 of the main text following the conventions of Ref. 62 (multiplied by a global minus sign and adapted to spinless fermions). The real part then is

$$\text{Re}\Pi_{F,1d}(\omega, Q) = -\frac{n}{\epsilon_F 4\tilde{Q}} \left(\log \left| \frac{1 + Q_-^2/(2\tilde{Q})}{1 - Q_-^2/(2\tilde{Q})} \right| - \log \left| \frac{1 + Q_+^2/(2\tilde{Q})}{1 - Q_+^2/(2\tilde{Q})} \right| \right), \quad (16)$$

with the abbreviations $Q_{\pm}^2 = \tilde{\omega} \pm \tilde{Q}^2$ where $\tilde{\omega} = \omega/\epsilon_F$ and $\tilde{Q} = Q/k_F$.

The imaginary part for $\tilde{Q} \geq 2$ is

$$\text{Im}\Pi_{F,1d}(\omega, Q) = \frac{n\pi}{\epsilon_F 4\tilde{Q}}, \quad (17)$$

if $\tilde{Q}^2 - 2\tilde{Q} \leq \tilde{\omega} \leq \tilde{Q}^2 + 2\tilde{Q}$ and zero otherwise.